




DOI: 10.34910/MCE.107.2

Behavior of RC beams with different bond strength

A. Alkhalwaldeh*, R. Al-Rousan 

Jordan University of Science and Technology, Irbid, Jordan

*E-mail: aalkhalwaldeh91@gmail.com

Keywords: materials science, civil engineering, structural, concrete, engineering

Abstract. This study investigates the impact of carbon fiber reinforced polymers (CFRP) composite to concrete bond strength degradation on the flexural response of CFRP strengthened reinforced concrete (RC) beams by using nonlinear finite element analysis (NLFEA). After reasonable validation of NLFEA simulated beams with the experimental test results of companion beams, NLFEA was expanded to provide a parametric study of twenty-two beams that correlates the ultimate flexural strength of RC beams to degradation in concrete compressive strength, degradation in bond strength, CFRP bond surface with concrete, and the number of layers and the size effect. The results show that the increase of CFRP-to-concrete contact area, concrete strength degradation, and epoxy bond strength degradation percentage had a significant impact on ultimate load capacity, ultimate deflection, stiffness, and energy absorption. Finally, new guidelines were proposed for designers and researchers to find the reduction in concrete strength as well as CFRP-to-concrete contact area at any ultimate load capacity of RC beams.

1. Introduction

The alarming deterioration of world's infrastructure has lead engineers to search for new techniques of rehabilitating deficient structures. The major reason of deterioration in concrete infrastructure facilities such as buildings, bridges, waterfront, marine constructions, and chemical plants is corrosion of steel reinforcement. Even though a variety of solutions like cathodic protection, epoxy coatings, polymer concrete, and increased concrete cover have been tried in the past, none of the procedures have provided long-term solutions. The construction industry is in ominous necessitate of alternative materials to steel, which do not corrode.

Concrete or steel jacketing considered as traditional strengthening techniques of existing deficient structures. Although these techniques are practicable and resolve just the strength issue, issues associated with them such as enlarge in the self-weight and strengthened member dimensions; the time necessary to carry out the strengthening work is moderately significant. In some situations, such as a bridge on a demanding highway or in issue of factories it may be complicated to take them out of service during application strengthening system. The consumption of advanced composite materials shows enormous possible in the area of structural rehabilitation. Composites offer several advantages in structural uses, such as lighter weights, higher strengths, design flexibility that enables the creation of complex and large shapes, and corrosion resistance. Other factors which call for the use of carbon fiber reinforced polymers (CFRP) composites in the strengthening and rehabilitation of deficient structures is tailor and time ability, CFRP strengthening techniques allow for cost-efficient retrofit alternative although the initial cost of CFRP composites is higher than traditional strengthening techniques. As a result, several papers on various aspects related to the paper subject have been published such as rehabilitation of damaged and deficient bridges and buildings [1–4], investigation the durability performance and safety factors of reinforced concrete (RC) beams [5–9], type of composite [10–11], severe conditions [12], type of loading [13], type of concrete [14–18], precast concrete [19], and low thermal transmittance [20].

Alkhalwaldeh, A., Al-Rousan, R. Behavior of RC beams with different bond strength. Magazine of Civil Engineering. 2021. 107(7). Article No. 10702. DOI: 10.34910/MCE.107.2

© Alkhalwaldeh, A., Al-Rousan, R., 2021. Published by Peter the Great St. Petersburg Polytechnic University.



This work is licensed under a CC BY-NC 4.0

Nonlinear Finite Element analysis (NLFEA) is an essential and efficient tool in the analysis and simulating of complex structures. The major benefits that NLFEA provided are: 1) significant savings in the time, cost, and effort compared with the experimental fabrication and testing of real structure elements, 2) freedom to modify any interest parameter to assess its influence on the structure, such as the strength of concrete in tension and compression, 3) and freedom to get the strain, stress, and displacement values at any load level and at any location. Recently, few researchers have attempted to simulate the complexity behavior of reinforced concrete externally strengthened with CFRP composites using NLFEA in the area of prestressed concrete [21–22], two-way slabs subjected to drop-weight [23], cable-stayed bridges [24], RC columns [25], thermal shock [26], bending and torsion [27], and hybrid FRP/steel technique [28]. Therefore, essential issues to produce effective, economical, and successful CFRP strengthening were discussed. Also, the impact of CFRP composite to concrete bond strength degradation on the flexural response of CFRP strengthened RC beams by using NLFEA received miniature consideration. The scientific problem considered in the study is indeed one of the problems in the modern theory of reinforced concrete. Despite a significant number of studies on the problem of bond between CFRP and concrete are limited to date. There are no sufficiently reliable solutions to this problem that most fully reflect the physical nature of the problem. In this study, the main subject is investigated the novel application in which was implemented in which the CFRP sheet was integrated as external flexural strengthening for RC beams. A lack of literature regarding the behavior of simply supported RC beams strengthened externally with CFRP composite and subjected to degradation in bond strength are necessitated conducting the present investigation. The main objectives of this study are to investigate the effect of CFRP contact area with concrete ($0.00A_t$, $0.25A_t$, $0.50A_t$, $0.75A_t$, and $1.00A_t$), concrete compressive strength (55, 51.6, 48.1, 44.7, 41.3, 37.8, 34.4, 30.9, 27.5, and 24.1 MPa), and epoxy bond strength degradation percentage (0, 15, 25, 35, 45, 55, 65, 75, and 85 %) in order to provide procedures and guidelines for researchers and designers.

2. Method

The goal of this analysis is to determine the effect of CFRP contact area with concrete, concrete compressive strength, and epoxy bond strength degradation percentage in the behavior of reinforced concrete (RC) flexural beams. Twenty-two beams were created analyzed in order to study the ultimate flexural strength of RC beams to degradation on concrete compressive strength, degradation in bond strength, CFRP bond surface with concrete, and number of layers.

2.1. Design constants

Twenty-two identical RC Strengthened beams with CFRP sheet layers were modelled using NLFEA. The cross section of all simulated beams is 150 mm × 250 mm with a length is 1200 mm. The beams were reinforced with three bars of $\phi 12$ at the bottom, two bars of $\phi 8$ bars at the top, and $\phi 8$ stirrups spaced at 75 mm on centers (Fig. 1).

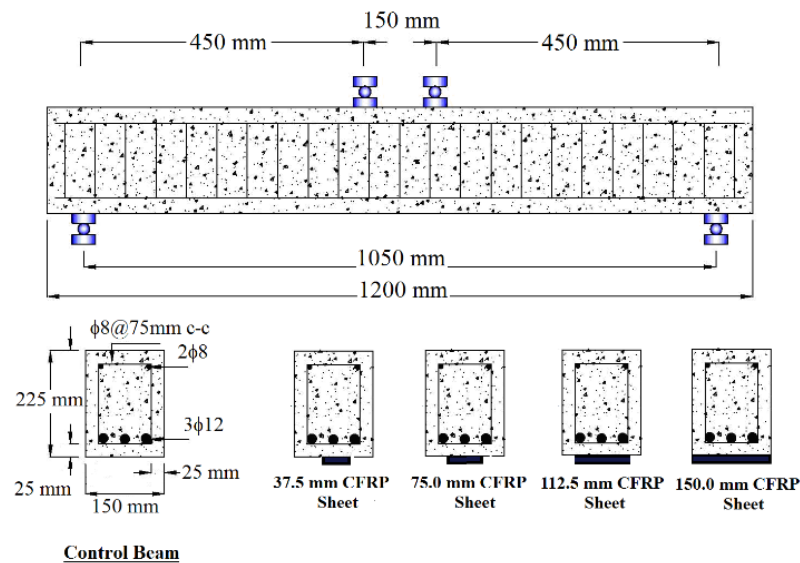


Figure 1. Typical layout of the simulated beams.

The first group includes five beams which simulated with different CFRP width (w_f) of 0 mm ($0.00A_t$), 37.5 mm ($0.25A_t$), 75 mm ($0.50A_t$), 112.5 mm ($0.75A_t$), and 150 mm ($1.00A_t$) to study the effect of CFRP contact area with concrete (Table 1). The second group includes ten control beams which simulated with different concrete compressive strength (f/c) of 55, 51.6, 48.1, 44.7, 41.3, 37.8, 34.4, 30.9, 27.5, and

24.1 MPa to study the degradation in concrete compressive strength (Table 2). The third group includes nine beams which simulated with different bond layer strength reduction percentage of 0, 15, 25, 35, 45, 55, 65, 75, and 85 % to study the epoxy bond strength degradation percentage (Table 3).

Table 1. Beams with different CFRP contact area.

Specimen	CFRP sheet width (w_f), mm	f'_c , MPa	Epoxy bond strength degradation (EBD), %	Ultimate deflection, mm (%)	Ultimate load, kN (%)	Stiffness, kN/mm (%)	Energy Absorption, kN.mm (%)
Bfc55wf0er0	0.0 (0.00 A_t)	55	0	40.0 (100)	170.5 (100)	26.2 (100)	5917 (100)
Bfc55wf37.5er0	37.5 (0.25 A_t)	55	0	38.8 (97)	180.8 (106)	29.7 (113)	6240 (105)
Bfc55wf75er0	75.0 (0.50 A_t)	55	0	37.5 (94)	192.7 (113)	32.6 (124)	6392 (108)
Bfc55wf112.5er0	112.5 (0.75 A_t)	55	0	36.1 (90)	201.7 (118)	35.4 (135)	6433 (109)
Bfc55wf150er0	150.0 (1.00 A_t)	55	0	34.5 (86)	207.7 (122)	38.4 (146)	6484 (110)

Note: A_t : Area of the tension side = length of the beam (L) × width of the beam (b)

Table 2. Beams with different concrete strength.

Specimen	CFRP sheet width (w_f), mm	f'_c , MPa	Epoxy bond strength degradation (EBD), %	Ultimate deflection, mm (%)	Ultimate load, kN (%)	Stiffness, kN/mm (%)	Energy Absorption, kN.mm (%)
Bfc55.0wf0er0	0.0 (0.00 A_t)	55.0	0	40.0 (100)	170.5 (100)	26.2 (100)	5917 (100)
Bfc51.6wf0er0	0.0 (0.00 A_t)	51.6	0	36.9 (92)	162.5 (95)	25.0 (91)	5192 (88)
Bfc48.1wf0er0	0.0 (0.00 A_t)	48.1	0	34.1 (85)	155.8 (91)	24.0 (87)	4533 (77)
Bfc44.7wf0er0	0.0 (0.00 A_t)	44.7	0	31.8 (79)	150.5 (88)	23.2 (84)	4077 (69)
Bfc41.3wf0er0	0.0 (0.00 A_t)	41.3	0	29.9 (75)	145.6 (85)	22.4 (81)	3735 (63)
Bfc37.8wf0er0	0.0 (0.00 A_t)	37.8	0	28.4 (71)	142.5 (84)	21.9 (79)	3455 (58)
Bfc34.4wf0er0	0.0 (0.00 A_t)	34.4	0	27.3 (68)	140.3 (82)	21.6 (78)	3246 (55)
Bfc30.9wf0er0	0.0 (0.00 A_t)	30.9	0	26.6 (67)	138.5 (81)	21.5 (77)	3085 (52)
Bfc27.5wf0er0	0.0 (0.00 A_t)	27.5	0	26.3 (66)	137.1 (80)	21.2 (76)	2998 (51)
Bfc24.1wf0er0	0.0 (0.00 A_t)	24.1	0	25.9 (65)	134.8 (79)	21.0 (75)	2883 (49)

Note: A_t : Area of the tension side = length of the beam (L) × width of the beam (b)

Table 3. Beams with different epoxy bond strength degradation percentage.

Specimen	CFRP sheet width (w_f), mm	f'_c , MPa	Epoxy bond strength degradation (EBD), %	Ultimate deflection, mm (%)	Ultimate load, kN (%)	Stiffness, kN/mm (%)	Energy Absorption, kN.mm (%)
Bfc55wf150er0	150.0 (1.00 A_t)	55.0	0	34.5 (100)	207.7 (100)	38.4 (100)	6484 (100)
Bfc55wf150er15	150.0 (1.00 A_t)	55.0	15	33.4 (97)	203.8 (98)	37.7 (93)	6148 (95)
Bfc55wf150er25	150.0 (1.00 A_t)	55.0	25	32.7 (95)	200.4 (96)	37.1 (92)	5904 (91)
Bfc55wf150er35	150.0 (1.00 A_t)	55.0	35	32.0 (93)	198.0 (95)	36.6 (91)	5708 (88)
Bfc55wf150er45	150.0 (1.00 A_t)	55.0	45	31.2 (90)	194.1 (93)	35.9 (89)	5449 (84)
Bfc55wf150er55	150.0 (1.00 A_t)	55.0	55	30.5 (88)	189.2 (91)	35.0 (87)	5189 (80)
Bfc55wf150er65	150.0 (1.00 A_t)	55.0	65	30.0 (87)	183.5 (88)	33.9 (84)	4950 (76)
Bfc55wf150er75	150.0 (1.00 A_t)	55.0	75	29.1 (84)	176.5 (85)	32.6 (81)	4598 (71)
Bfc55wf150er85	150.0 (1.00 A_t)	55.0	85	27.9 (81)	172.2 (83)	31.8 (79)	4287 (66)

Note: A_t : Area of the tension side = length of the beam (L) × width of the beam (b)

2.2. Elements

The concrete material was modelled by using SOLID65 which can be used for the 3-D modelling of solids with or without steel reinforcing bars. SOLID65 is eight nodes element with three degrees of freedom at each node with translations in the nodal x, y, and z directions. The most significant aspects of SOLID65

are the conducting of nonlinearity of concrete material and capable of crushing, cracking (in three orthogonal directions), creep, and plastic deformation. The steel reinforcement bars were modelled by using LINK8 element (3-D spar element) with a uniaxial compression-tension element with three degrees of freedom at each node with translations in the nodal x, y, and z directions. Steel plates at the supports and load applications were modelled by using SOLID45 in the models with eight nodes having three degrees of freedom at each node with 8 translations in the nodal x, y, and z directions. Finally, CFRP composite sheet was modelled by using SOLID46 (layered element of the 8-node structural solid) which allows up to 250 different material layers with different orthotropic material properties and orientations in each layer. SOLID46 has three degrees of freedom at each node with translations in the nodal x, y, and z directions. Fig. 2 shows the types of used elements used in the NLFEA simulated beams.

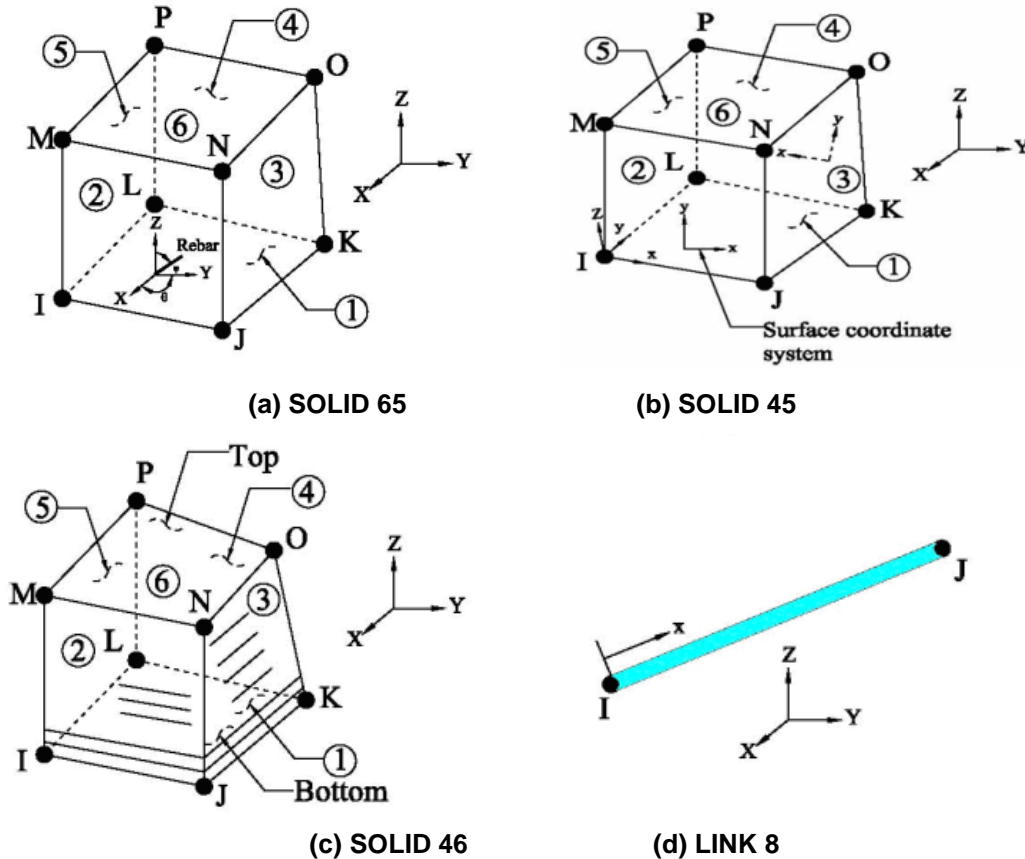


Figure 2. Types of the used elements used in the NLFEA.

2.3. Materials

Concrete material is classified as quasi-brittle material with different performance in tension and compression. The used SOLID65 element can predict the nonlinear performance of concrete materials via a smeared crack approach which predicts concrete material failure and accounts for both crushing and cracking failures. Therefore, the main two input strength parameters required to define a failure surface for the concrete material are ultimate uniaxial compressive and tensile strengths. As a result, a failure criterion of concrete due to a multi axial stress state should be calculated [31]. In addition, a Poisson's ratio of 0.2 was used for all simulated beams. The conditions of the crack face can be represented by shear transfer coefficient (β_t). Generally, the β_t value ranges from 0.0 (a smooth crack with complete loss of shear transfer) to 1.0 (a rough crack with no loss of shear transfers). The β_t value ranges from 0.05 to 0.25 was used in many studies of reinforced concrete structures [31]. Thus, a β_t value of 0.2 was used in this study. The concrete properties include f'_c of 55, 51.6, 48.1, 44.7, 41.3, 37.8, 34.4, 30.9, 27.5, and 24.1 MPa, initial young's modulus (E_c) of 34856, 33762, 32596, 31423, 30205, 28896, 27566, 26126, 24647, and 23073 MPa, respectively. In tension stage, the concrete stress-strain curve is assumed to be linearly elastic up to the ultimate strength. After this limit, the concrete started to crack and the strength decreases to zero. Figure 3(a) shows the concrete simplified uniaxial stress-strain relationship that is used in this study for f'_c of 55 MPa.

The steel reinforcement bars for the simulated models was assumed to be an elastic-perfectly plastic material with the same properties in compression and tension as shown in Fig. 3 (b). Yield stress and

Poisson's ratio of 413 MPa and 0.3, respectively were used for defining the steel reinforcement bars. A more even stress distribution over the support areas were provided by adding steel plates at both ends of the beams. The performance steel plates were assumed to be linear elastic materials with Poisson's ratio of 0.3 and an elastic modulus of 200 GPa.

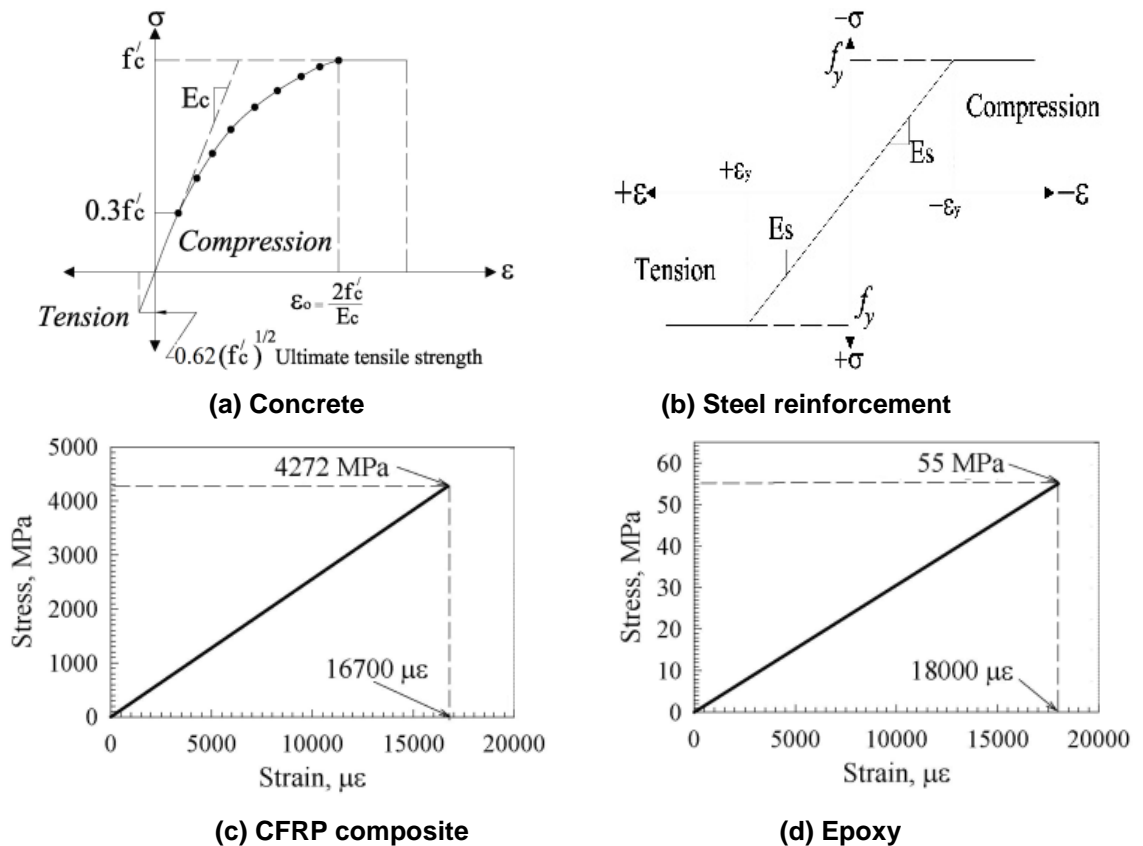


Figure 3. Stress-strain curves: (a) concrete, (b) steel Reinforcement, (c) CFRP composite sheet, and (d) epoxy.

The CFRP composite sheet is assumed an orthotropic material of tensile strength of 3790 MPa, 0.165 mm thick, ultimate tensile strain of 0.017 in/in, and elastic modulus of 228 GPa as shown in Fig. 3(c). The epoxy material is assumed an isotropic material of ultimate tensile strength 55 MPa, 0.343 mm thick, ultimate tensile strain of 0.018 mm/mm, and elastic modulus of 30 GPa as shown in Fig. 3(d). The elastic modulus of CFRP composite sheet was assumed to be 10^{-6} times that of the main direction for the other directions perpendicular to the fibre direction. Linear elastic property performance was assumed for both CFRP composite sheet and epoxy.

2.4. Models

Quarter of the simulated beam with appropriate boundary conditions was used in the NLFEA simulation by taking advantage of the symmetry in the reinforced concrete beam configuration and the applied loading. This advantage can reduce the computer disk space requirements and computational time. The appropriate mesh density was determined by carried a convergence study. Fig. 4 shows the finite element meshing of quarter of the RC beam. Perfect bond was assumed between the concrete and steel reinforcement epoxy as well as between CFRP composite sheet and epoxy. Close up views of appropriate boundary conditions and finite element meshing of the beams is shown in Fig. 5.

The applied load was divided into a series of load steps or load increments. Convergence at the end of each load increment within tolerance limits is equal to 0.001 which is provided by Newton–Raphson equilibrium iterations. The maximum and minimum load step sizes were automated by ANSYS program. The cracking created when the principal tensile stress in any direction occurred outside the failure surface of concrete. After creation of crack, the concrete elastic modulus is set to zero in the direction parallel to the direction of principal tensile stress. Crushing occurs when all compressive principal stresses are lies outside the failure surface of concrete, afterwards, the elastic modulus is set to zero in all directions, and the element efficiently disappears. The simulated finite element model fails impetuously when the crushing concrete capability is turned on. Concrete crushing started to grow in elements situated directly under the load locations and significantly reducing the local stiffness. Ultimately, the simulated model showed a large displacement and the solution diverged. Consequently, the concrete crushing capability was turned off and

concrete cracking inhibited the failure of the simulated finite element models. The loads were applied steadily with smaller load increments at concrete cracking and ultimate load stages. Failure for each simulated model was recognized when the solution for 0.0045 kN load increment was not converging.

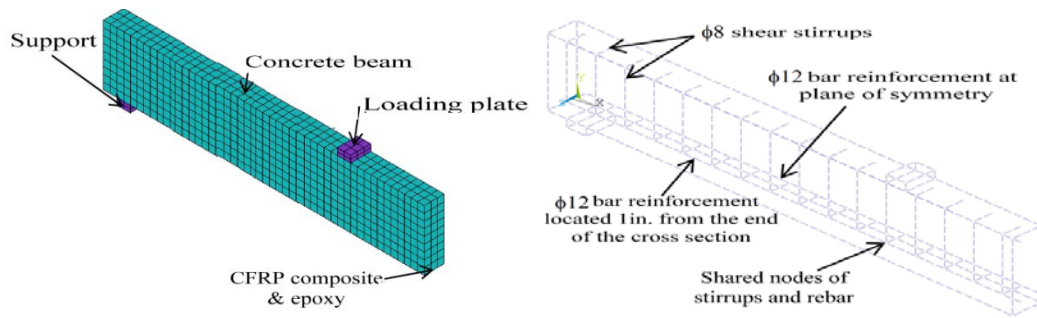


Figure 4. Typical finite element meshing of quarter of the beam.

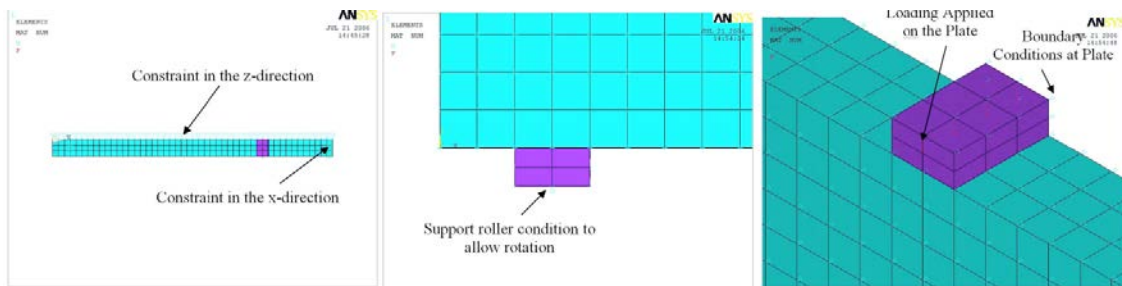


Figure 5. Close up view of the finite element meshing of the beams and boundary conditions.

3. Results and Discussion

3.1. Validation of models

Fig. 6 shows the load deflection response of the NLFEA simulated beams and tested beams reported by Al-Rousan and Issa [12]. The load-deflection response of CFRP strengthened beams, as with the virgin (control) beams, was linear behaviour until the creation of the flexural cracks as well as the main steel reinforcement is starting to yield. After the steel reinforcement yielding point, the deflection increased rapidly with tiny reduction in ultimate load capacity. Also, the CFRP sheets had a significant impact on the ultimate load capacity and corresponding deflection as well as redistribution of stresses occurred and thus increasing the beam's strength at yielding. In comparison with the control beams, the load-deflection performance of the CFRP strengthened beams was enhanced by the addition of CFRP sheets as indicated by the enhancement of the ultimate load capacity, and the reduction in the corresponding deflection at any load level. Inspection of Fig. 6 reveals that there is a good agreement between the NLFEA simulated beams and the experimental test results in terms of ultimate strength and load response. Fig. 7 shows a typical NLFEA deformed shape deformed of control beam and stress contours of concrete beam externally strengthened with one layer of CFRP composites.

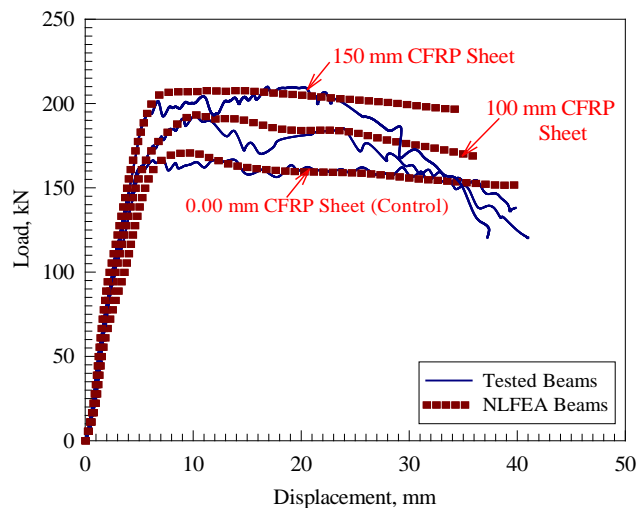


Figure 6. Load-deflection curve of NLFEA and tested beams [12].

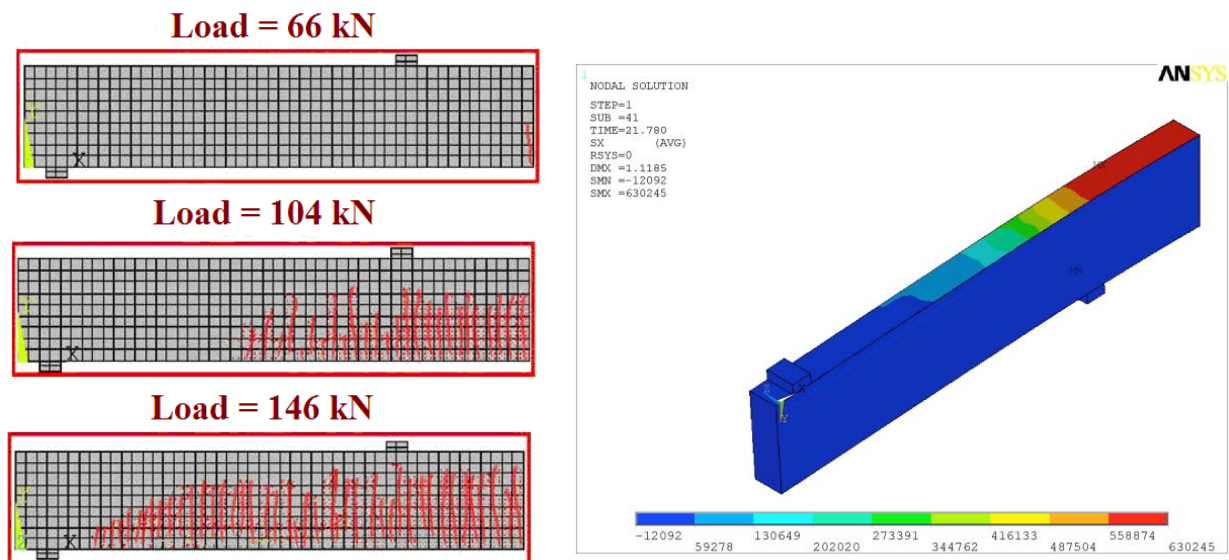


Figure 7. Typical NLFEA (a) deformed shape of control beam and (b) stress contours of 1 layers CFRP beam.

3.2. Effect of CFRP contact area

Table 1 shows the effect of CFRP contact area with concrete for beams strengthened with CFRP contact area of 0 CFRP sheet layer ($0.00A_t$), 0.25 CFRP sheet layer ($0.25A_t$), 0.50 CFRP sheet layer ($0.50A_t$), 0.75 CFRP sheet layer ($0.75A_t$), and 1.00 CFRP sheet layer ($1.00A_t$) for w_f of 0 mm, 37.5 mm, 75 mm, 112.5 mm, and 150 mm, respectively, and concrete compressive strength of 55 MPa. Inspection of Table 1 reveals that the enhancement ultimate capacity strength of beams strengthened 0.25 CFRP sheet layer ($0.25A_t$), 0.50 CFRP sheet layer ($0.50A_t$), 0.75 CFRP sheet layer ($0.75A_t$), and 1.00 CFRP sheet layer ($1.00A_t$) with respect to control beam was 6 %, 13 %, 18 %, and 22 %, respectively. Whereas, the deflection of the strengthened beams decreased with the increase of CFRP contact area with a reduction percentage of 3 %, 6 %, 10 %, and 14 % for 0.25 CFRP sheet layer, 0.50 CFRP sheet layer, 0.75 CFRP sheet layer, and 1.00 CFRP sheet layer, respectively. The stiffness scored the maximum enhancement percentage of 13%, 24 %, 35 %, and 46 % for 0.25 CFRP sheet layer, 0.50 CFRP sheet layer, 0.75 CFRP sheet layer, and 1.00 CFRP sheet layer, respectively, which is almost twice the enhancement in the ultimate capacity strength. While, the energy absorption scored the minimum enhancement percentage of 5 %, 8 %, 9 %, and 10 % for 0.25 CFRP sheet layer, 0.50 CFRP sheet layer, 0.75 CFRP sheet layer, and 1.00 CFRP sheet layer, respectively, which is almost one third of the enhancement in the stiffness. As a result, when the CFRP contact area increased 100 % of beam strengthened with CFRP sheet layer (150 mm contact area with concrete) with respect to the control beam strengthened, the ultimate flexural strength, stiffness, and energy absorption increased 22 %, 46 %, and 10 %, respectively. Fig. 8 shows the load deflection response of the NLFEA simulated beams with different CFRP contact area. Inspection of Fig. 8 reveals that the load-deflection response can be divided into two stages. The first stage represents the linear part from zero loading up to yielding of the steel reinforcement bars in which the load was carried by steel reinforcement. Then, the second stage represents almost a linear part with tiny reduction in ultimate load capacity and large increasing in deflection in which the load was carried by CFRP sheet.

Fig. 9 shows the effect of CFRP contact area on the CFRP delamination profile of beams strengthened with different configuration. Inspection of Fig. 9 reveals that the initial CFRP sheet delamination length of the beams strengthened decreased with the increase of CFRP contact area in which the CFRP sheet delamination length is 250 mm (2.5 times the CFRP sheet delamination length of the beam strengthened with 1.00 CFRP sheet layer), 200 mm (2 times the CFRP sheet delamination length of the beam strengthened with 1.00 CFRP sheet layer), 150 mm (1.5 times the CFRP sheet delamination length of the beam strengthened with 1.00 CFRP sheet layer), and 100 mm for 0.25 CFRP sheet layer, 0.50 CFRP sheet layer, 0.75 CFRP sheet layer, and 1.00 CFRP sheet layer, respectively.

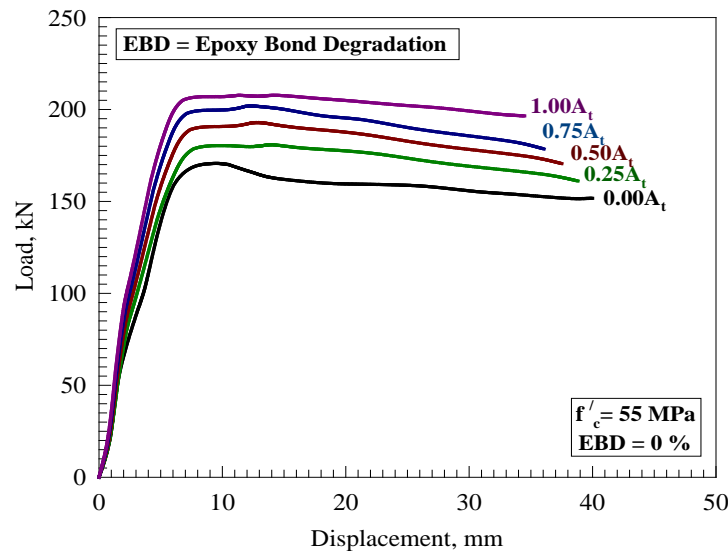


Figure 8. Load-deflection curve of beams with different CFRP contact area.

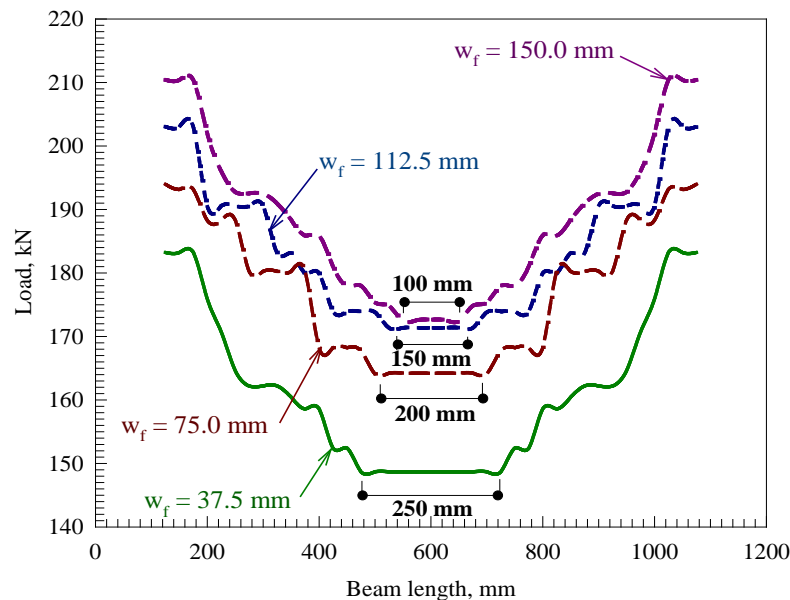


Figure 9. CFRP delamination profile of beams with different CFRP contact area.

3.3. Effect of concrete strength degradation

Fig. 10 shows the load deflection response of the NLFEA simulated beams with different concrete strength. Inspection of Fig. 10 reveals that the load-deflection response can be also divided into two stages. The first stage represents the linear part from zero loading up to yielding of the steel reinforcement bars in which the load was carried by steel reinforcement. Then, the second stage represents a descending linear part from yielding of the steel reinforcement bars up to failure with slope increase with the decrease of concrete strength.

Table 2 shows the effect of concrete strength for control beams with f/c of 55, 51.6, 48.1, 44.7, 41.3, 37.8, 34.4, 30.9, 27.5, and 24.1 MPa. Inspection of Table 2 reveals that the reduction in ultimate capacity strength of control beams with f/c of 55, 51.6, 48.1, 44.7, 41.3, 37.8, 34.4, 30.9, 27.5, and 24.1 MPa was 5 %, 9 %, 12 %, 15 %, 16 %, 18 %, 19 %, 20 % and 21 %, respectively. Whereas, the reduction in deflection of the control beams is almost 1.5 times the reduction in ultimate capacity strength. The reduction in stiffness is almost the same the reduction in ultimate capacity strength. While, the energy absorption scored the maximum reduction percentage of 12 %, 23 %, 31 %, 37 %, 42 %, 45 %, 48 %, 49 % and 51 %, for f/c of 55, 51.6, 48.1, 44.7, 41.3, 37.8, 34.4, 30.9, 27.5, and 24.1 MPa, respectively, which is almost twice the reduction in the ultimate capacity strength.

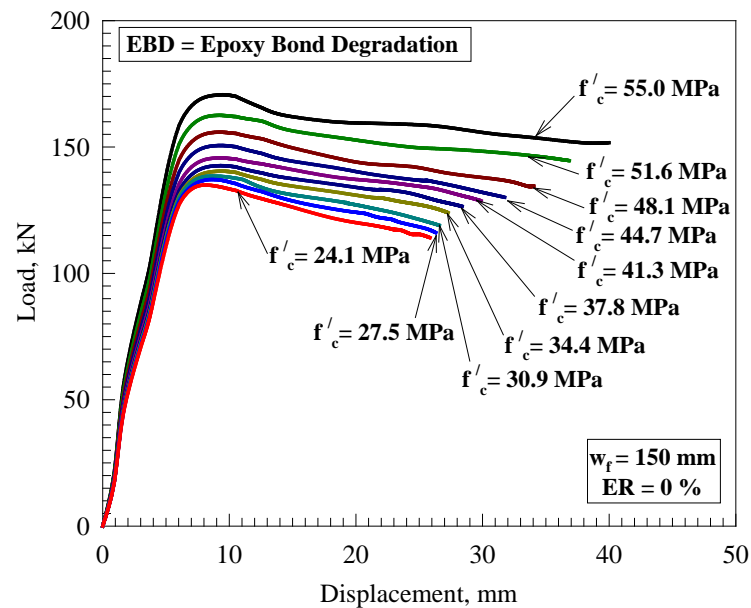


Figure 10. Load-deflection curve of beams with different concrete strength.

Table 4 shows the ultimate flexural load capacity of CFRP strengthened reinforced concrete beams exposed for three years for the room temperature, cyclic ponding in 15 % salt-water solution, hot-water of 65 °C, and rapid freeze/thaw cycles reported by Al-Rousan and Issa [12]. Fig. 11 shows that the damage percentage in concrete had a parabolic relation with the ultimate strength of control beams. Inspection of Fig. 11 reveals that the damage percentage in concrete strength of freeze and thaw beams of 166.8 kN ultimate load capacity was 3.2 % (53.2 MPa) which almost 2 times the reduction in ultimate load capacity with respect to the control beam under room temperature. Also, the damage percentage of the salt and hot water beams was 4.8 % (31.7 MPa) and 23.0 % (42.4 MPa), respectively, which corresponded to almost 2 times the reduction in ultimate load capacity with respect to the control beam under room temperature. In the real life, the beams always subject under more than two conditions and sometimes all the conditions. Therefore, the damage percentage for the beams subjected to freeze-thaw and salt water cycles by using the experimental results reported by Al-Rousan and Issa [12] was 8 % (50.6 MPa) as shown in Fig. 11. The damage percentage for the beams subjected to hot and salt water cycles was 26.7% (40.2 MPa). For all conditions, the damage percentage was 29 % (39.1 MPa) as shown in Fig. 11. As a result, Fig. 11 provided guidelines for designers and researchers to find the reduction in concrete strength at any ultimate load capacity of RC beams.

Table 4. The details of the tested beam specimens [12].

Group	Beam Designation	Type of strengthening with CFRP	Ultimate load, kN
I (Room Temperature)	BRC0	Unstrengthened (control)	169.9
	BRC1	1-layer Sheet	211.3
II (Freeze and Thaw)	BFC0	Unstrengthened	166.8
	BFC1	1-layer Sheet	202.8
III (Heat Tank Water)	BHC0	Unstrengthened	147.2
	BHC1	1-layer Sheet	186.4
IV (Ponding Salt Water)	BSC0	Unstrengthened	165.0
	BSC1	1-layer Sheet	198.8

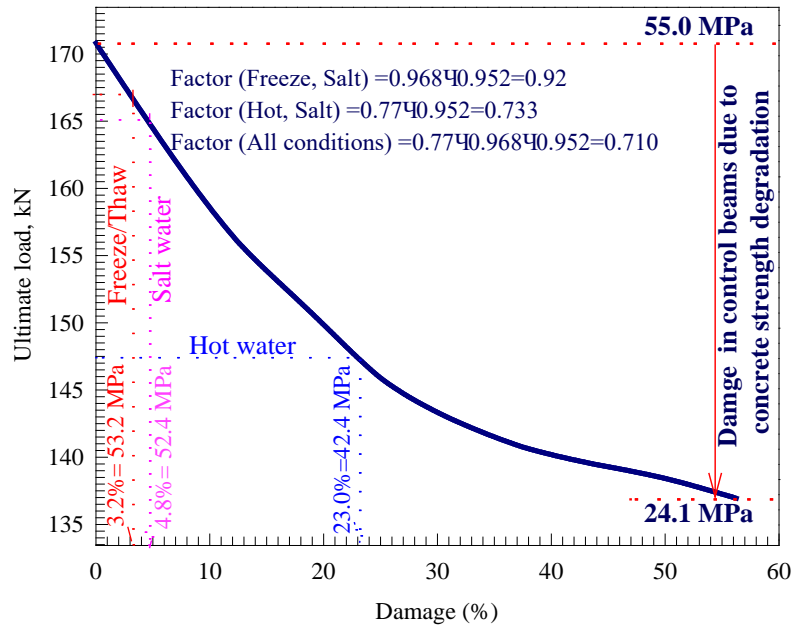


Figure 11. Damage percentages versus ultimate load capacity of control beam.

3.4. Effect of epoxy bond strength degradation

Fig. 12 shows the load deflection response of the NLFEA simulated beams with different epoxy bond strength degradation percentage. Inspection of Fig. 12 reveals that the load-deflection response can be also divided into two stages. The first stage represents the linear part from zero loading up to yielding of the steel reinforcement bars in which the load was carried by steel reinforcement. Then, the second stage represents almost a liner part with small reduction in ultimate load capacity and large increasing in deflection in which the load was carried by CFRP sheet. Also, Fig. 12 shows that the area under the curve as well as the ultimate ductility decreased with the increase of epoxy bond strength degradation percentage.

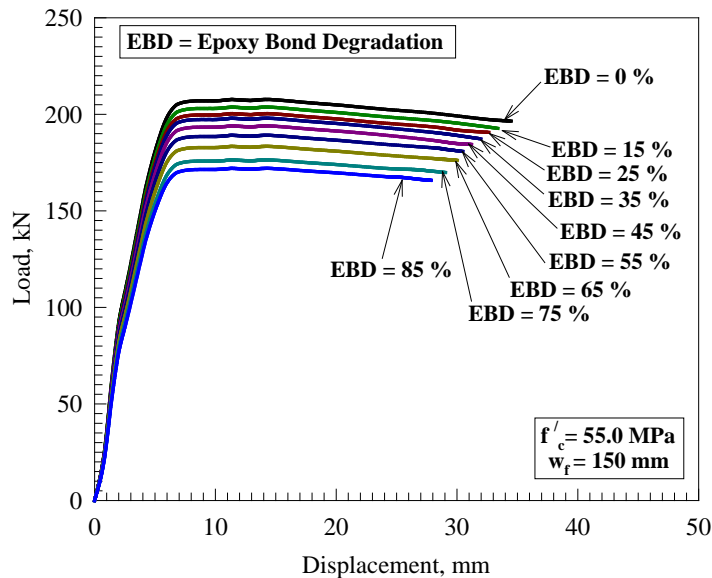


Figure 12. Load-deflection curve of beams with different epoxy bond strength degradation percentage.

Fig. 13 shows the effect of epoxy bond strength degradation percentage on the CFRP delamination profile. Inspection of Fig. 13 reveals that the initial CFRP sheet delamination length of the beams strengthened increased with the increase of epoxy bond strength degradation percentage. Fig. 13 shows that the increase in CFRP sheet delamination length of strengthened beams is 11 %, 16 %, 21 %, 26 %, 32 %, 42 %, 53 %, 63 %, and 79 % of the CFRP bonded length for epoxy bond strength degradation percentage of 0 %, 15 %, 25 %, 45 %, 55 %, 65 %, 75 %, and 85 %, respectively. As a result, the increase in CFRP sheet delamination length of strengthened beams is almost equal to an average percentage of 83 % of epoxy bond strength degradation percentage.

Table 3 shows the effect of epoxy bond strength degradation percentage for CFRP strengthened beams with f/c of 55. Inspection of Table 3 reveals that the reduction in ultimate capacity strength with respect to CFRP strengthened beam without reduction in epoxy bond strength was 3 %, 5 %, 7 %, 10 %, 12 %, 13 %, 16 %, and 19 % for EBD of 15 %, 25 %, 45 %, 55 %, 65 %, 75 %, and 85 %, respectively. Whereas, the reduction in deflection of the CFRP strengthened beams is almost 0.95 times the reduction in ultimate capacity strength. The reduction in stiffness is almost 1.05 times the reduction in ultimate capacity strength. While, the energy absorption scored the maximum reduction percentage of 5 %, 9 %, 12 %, 16 %, 20 %, 24 %, 29 %, and 34 % for EBD of 15 %, 25 %, 45 %, 55 %, 65 %, 75 %, and 85 %, respectively, which is almost twice the reduction in the ultimate capacity strength.

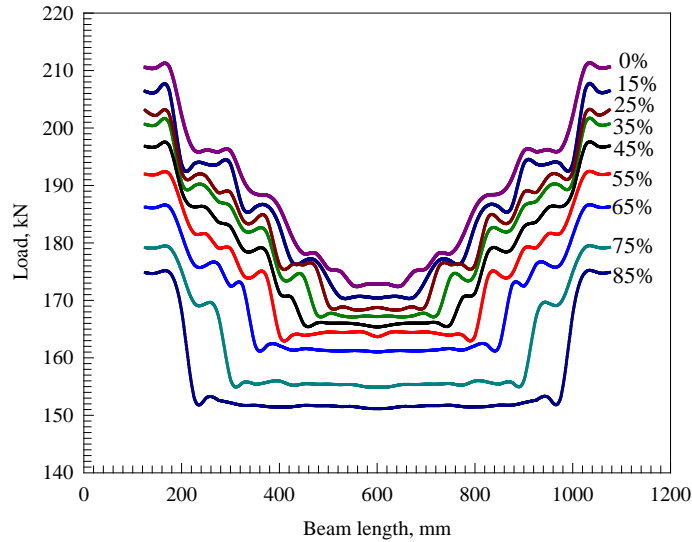


Figure 13. CFRP delamination profile of beams with different epoxy bond strength degradation percentage.

Fig. 14 shows bond strength degradation on ultimate load capacity. Inspection of Fig. 14 reveals that the bond strength degradation of freeze and thaw beams of 166.8 kN ultimate load capacity was 18 % which almost 10 times the reduction in ultimate load capacity with respect to the beam under room temperature. Also, the bond strength degradation of the salt and hot water beams was 24 % and 35 %, respectively, which corresponded to almost 9 times and 3 times the reduction in ultimate load capacity with respect to the beam under room temperature. For the beam subjected to freeze-thaw and salt water cycles, the bond strength degradation was 37.6 %. For the beam subjected to hot and salt water cycles, the bond strength degradation was 50.6 %. For all conditions, the bond strength degradation was 59.6 % as shown in Fig. 14. As a result, Fig. 14 provided guidelines for designers and researchers to find the bond strength degradation at any ultimate load capacity or RC beams.

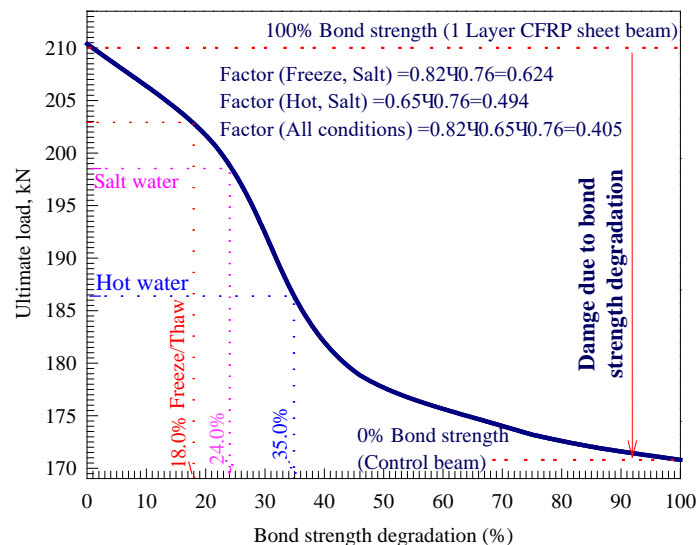


Figure 14. Bond strength degradation versus ultimate load capacity of control beam.

4. Conclusions

1. The load deflection response of the NLFEA simulated beams can be divided into two stages. The first stage represents the linear part from zero loading up to yielding of the steel reinforcement bars in which the load was carried by steel reinforcement. Then, the second stage represents a descending linear part from yielding of the steel reinforcement bars up to failure with decreased slope based on the investigated parameters.

2. The increasing of CFRP contact area of beam strengthened with CFRP sheet layer (150 mm contact area with concrete) with respect to the control beam strengthened, the ultimate flexural strength, stiffness, and energy absorption increased 22 %, 46 %, and 10 %, respectively.

3. The ultimate capacity strength of control beams decreased with the decrease of concrete strength. Whereas, the reduction in deflection of the control beams is almost 1.5 times the reduction in ultimate capacity strength. The reduction in stiffness is almost the same the reduction in ultimate capacity strength. While, the energy absorption scored the maximum reduction percentage of twice the reduction in the ultimate capacity strength.

4. The epoxy bond strength degradation percentage decreased the ultimate capacity strength with respect to CFRP strengthened beam. Whereas, the reduction in deflection of the CFRP strengthened beams is almost 0.95 times the reduction in ultimate capacity strength. The reduction in stiffness is almost 1.05 times the reduction in ultimate capacity strength. While, the energy absorption reduction percentage is almost twice the reduction in the ultimate capacity strength.

5. The damage in ultimate flexural load capacity of control beam subjected to freeze-thaw and salt water, hot and salt water cycles, and freeze-thaw and salt water and hot water cycles (all conditions) was 8 %, 26.7 %, and 29 %, respectively.

6. The damage in bond strength of reinforced concrete beam externally strengthened with 1 layer of CFRP composites subjected to freeze-thaw and salt water, hot and salt water cycles, and freeze-thaw and salt water and hot water cycles (all conditions) was 37.6 %, 50.6 %, and 59.6 %, respectively.

7. New guidelines were proposed for designers and researchers to find the reduction in concrete strength as well as CFRP to concrete contact area at any ultimate load capacity of RC beams.

References

1. Meier, U. Carbon Fiber-Reinforced Polymers: Modern Materials in Bridge Engineering. Structural Engineering International. 1992. 2(1). Pp. 7–12. DOI: 10.2749/101686692780617020
2. Durability Evaluation of Carbon Fiber-Reinforced Polymer Strengthened Concrete Beams: Experimental Study and Design. ACI Structural Journal. 2005. 102(1). Pp. 40–53. DOI: 10.14359/13529
3. Wenwei, W., Guo, L. Experimental study of RC beams strengthened with CFRP sheets under sustaining loads. Journal of Wuhan University of Technology-Mater. Sci. Ed. 2006. 21(3), Pp. 82–85. DOI: 10.1007/bf02840887
4. Benjeddou, O., Ouezdou, M.B., Bedday, A. Damaged RC beams repaired by bonding of CFRP laminates. Construction and Building Materials. 2007. 21(6). Pp. 1301–1310. DOI: 10.1016/j.conbuildmat.2006.01.00
5. Ekenel, M., Myers, J.J. Durability performance of RC beams strengthened with epoxy injection and CFRP fabrics. Construction and Building Materials. 2007. 21(6). Pp. 1182–1190. DOI: 10.1016/j.conbuildmat.2006.06.020
6. Almusallam, T.H. Load-deflection behavior of RC beams strengthened with GFRP sheets subjected to different environmental conditions. Cement and Concrete Composites. 2006. 28(10). Pp. 879–889. DOI: 10.1016/j.cemconcomp.2006.07.017
7. Tan, K.H., Saha, M.K., Liew, Y.S. FRP-strengthened RC beams under sustained loads and weathering. Cement and Concrete Composites. 2009. 31(5). Pp. 290–300. DOI: 10.1016/j.cemconcomp.2009.03.002
8. Ji, G., Li, G., Alaywan, W. A new fire resistant FRP for externally bonded concrete repair. Construction and Building Materials. 2013. 42(1). Pp. 87–96. DOI: 10.1016/j.conbuildmat.2013.01.008
9. Trentin, C., Casas, J.R. Safety factors for CFRP strengthening in bending of reinforced concrete bridges. Composite Structures. 2015. 128(1). Pp. 188–198. DOI: 10.1016/j.compstruct.2015.03.048
10. Ferrari, V.J., de Hanai, J.B., de Souza, R.A. Flexural strengthening of reinforcement concrete beams using high performance fiber reinforcement cement-based composite (HPFRCC) and carbon fiber reinforced polymers (CFRP). Construction and Building Materials. 2013. 48(1). Pp. 485–498. DOI: 10.1016/j.conbuildmat.2013.07.026
11. Attari, N., Amziane, S., Chemrouk, M. Flexural strengthening of concrete beams using CFRP, GFRP and hybrid FRP sheets. Construction and Building Materials. 2012. 37(1). Pp. 746–757. DOI: 10.1016/j.conbuildmat.2012.07.052
12. Al-Rousan, R.Z., Issa, M.A. Flexural behavior of RC beams externally strengthened with CFRP composites exposed to severe environment conditions. KSCE Journal of Civil Engineering. 2016. 21(6). Pp. 2300–2309. DOI: 10.1007/s12205-016-0570-x
13. Kolchunov, V.I., Dem'yanov, A.I. The modeling method of discrete cracks in reinforced concrete under the torsion with bending. Magazine of Civil Engineering. 2018. 81(5). Pp. 160–173. DOI: 10.18720/MCE.81.16
14. Travush, V.I., Konin, D.V., Krylov, A.S. Strength of reinforced concrete beams of high-performance concrete and fiber reinforced concrete. Magazine of Civil Engineering. 2018. No. 77(1). Pp. 90–100. DOI: 10.18720/MCE.77.8
15. Usanova, K., Barabanshchikov, Yu., Fedorenko, Yu., Kostyrya, S. Cold-bonded fly ash aggregate as a coarse aggregate of concrete. Construction of Unique Buildings and Structures. 2018. 9(72). Pp. 31–45. DOI: 10.18720/CUBS.72.2

16. Volkova, A., Rybakov, V., Seliverstov, A., Petrov, D., Smignov, A. Strength characteristics of foam concrete samples with various additives. MATEC Web of Conferences 245, 03015 (2018). doi.org/10.1051/mateconf/201824503015
17. Volkova, A., Rybakov, V., Seliverstov, A., Petrov, D., Smignov, A. Lightweight steel concrete structures slab panels load-bearing capacity. MATEC Web of Conferences 245, 08007 (2018). doi.org/10.1051/mateconf/201824508008
18. Rybakov, V.A., Kozinetc, K.G., Vatin, N.I., Velichkin, V.Z., Korsun, V.I. Lightweight steel concrete structures technology with foam fiber-cement sheets. Magazine of Civil Engineering. 2018. 82(6). Pp. 103–111. DOI: 10.18720/MCE.82.10
19. Vatin, N.I., Velichkin, V.Z., Kozinetc, G.L., Korsun, V.I., Rybakov, V.A., Zhuvak, O.V. Precast-monolithic reinforced concrete beam-slabs technology with claydit blocks. Construction of Unique Buildings and Structures. 2018. 70(7). Pp. 43–59. DOI: 10.18720/CUBS.70.4
20. Barabanshchikov, Y., Fedorenko, I., Kostyrya, S., Usanova, K. Cold-Bonded Fly Ash Lightweight Aggregate Concretes with Low Thermal Transmittance: Review. Advances in Intelligent Systems and Computing. 2019. 983(1). Pp. 858–866. DOI: 10.1007/978-3-030-19868-8_84
21. Bily, P., Fladr, J., Kohoutkova, A. Finite Element Modelling of a Prestressed Concrete Containment with a Steel Liner. Proceedings of the Fifteenth International Conference on Civil, Structural and Environmental Engineering Computing. Civil-Comp Press. 2015. DOI: 10.4203/ccp.108.1
22. Bílý, P., Kohoutková, A. Sensitivity analysis of numerical model of prestressed concrete containment. Nucl. Eng. Des. 2015. 295(1). Pp. 204–214. DOI: 10.1016/j.nucengdes.2015.09.027
23. Al-Rousan, R. Behavior of two-way slabs subjected to drop-weight. Magazine of Civil Engineering. 2019. 90(6). Pp. 62–71. DOI: 10.18720/MCE.90.6
24. Al-Rousan, R. The impact of cable spacing on the behavior of cable-stayed bridges. Magazine of Civil Engineering. 2019. 91(7). Pp. 49–59. DOI: 10.18720/MCE.91.5
25. Mirmiran, A., Shahawy, M. Behavior of Concrete Columns Confined by Fiber Composites. Journal of Structural Engineering. 1997. 123(5). Pp. 583–590. DOI: 10.1061/(asce)0733-9445(1997)123:5(583)
26. Al-Rousan, R. Behavior of strengthened concrete beams damaged by thermal shock. Magazine of Civil Engineering. 2020. 94(2). Pp. 93–107. DOI: 10.18720/MCE.94.2
27. Al-Rousan, R., Abo-Msamh, I. Bending and Torsion Behaviour of CFRP Strengthened RC Beams. Magazine of Civil Engineering. 2019. 92(8). Pp. 42–51. DOI: 10.18720/MCE.92.8
28. Kara, I.F., Ashour, A.F., Körog'lu, M.A. Flexural behavior of hybrid FRP/steel reinforced concrete beams. Composite Structures. 2015. 129(1). Pp. 111–121. DOI: 10.1016/j.compstruct.2015.03.073

Contacts:

Ayah Alkhaldeh, aalkhaldeh91@gmail.com

Rajai Al-Rousan, rzalrousan@just.edu.jo